Daagu International Journal of Basic and Applied Research 5(2023): 193-208
DOI: https://doi.org/10.20372/DIJBAR.95607

Original article

Study of Organometallic Sensitizer Regeneration Kinetics by Scanning Electrochemical Microscopy

Ataklti Abraha Gebreyohanes [*1] and Getachew Alemu Anshebo [1]

College of Natural and Computational Sciences, Department of Physics, Samara University, Samara, Ethiopia, B.O.Box 132.

*Corresponding author: atklt.physics@gmail.com

Abstract

Organometallic perovskite is used as a sensitizer for nanoporous nickel oxide films in photoelectrochemical solar cell applications. The regeneration kinetics of light-absorbing sensitizer molecules by the organic electrolyte 1-methy-1H-tetrazole-5-thiolate (T^-) were studied using scanning electrochemical microscopy's feedback mode (SECM). The approach curves were used to calculate the regeneration rate constants. The rate constants (k_{red}) for perovskite and organic dye have been found as 9.98×10^6 $mol^{-1}cm^3s^{-1}$ and 4.51×10^5 $mol^{-1}cm^3s^{-1}$ respectively. Similarly, The absorption cross section (Φ_{hv}), for perovskite and organic dye have been found as 6.87×10^6 mol cm^2 for blue LED and 4.89×10^6 mol cm^2 for red LED, and 3.56×10^5 mol cm^2 for blue LED and 2.15×10^5 mol cm^2 for red LED respectively. Thus, we observed that regeneration parameters of organometallic perovskite were higher than organic dye. Generally, SECM investigation opens a new outlook for p-type dye-sensitized solar cell characterization.

Keywords: Organometallic Perovskite, SECM, Regeneration Parameters, Dye-Sensitized Solar Cells, Organic Dye.

Citation: Abraha, A. and Alemu, G. 2023. Study of Organometallic Sensitizer Regeneration Kinetics by Scanning Electrochemical Microscopy. *Daagu International Journal of Basic and Applied Research*, 5(1):193-208. DOI: https://doi.org/10.20372/DIJBAR.95607.

1. INTRODUCTION

Dyes-sensitized solar cells (DSSCs) have emerged as an economically feasible alternative to p-n junction photovoltaic devices. Light will therefore be transformed into electricity by the electron injection of excited dye molecules into a semiconductor's wide band gap (Tributsch & Calvin, 1971). Michael Grätzel and Brian O'Regan devised the dye-sensitized solar cell (DSSC) in 1991 as an alternative solar cell (Grätzel, 2003; Hagfeldt & Graetzel, 1995; Haque et al., 2005; O'regan & Grätzel, 1991). In recent decades, nanoscale dye-sensitized solar cells of TiO_2 and ZnO with various nanostructures of photoanodes DSSC have been explored. Dye-sensitized solar cells, based on iodide/triiodide liquid electrolytes, are a newly emerging photovoltaic technology for commercialization, with power conversion efficiencies exceeding 11% (Chen et al., 2009; Wang, Grätzel, Zakeeruddin, & Grätzel, 2012; Yella et al., 2011). Recent attempts to replace I_3^-/I^- have led to remarkable achievements (Mathew et al., 2014; Mora-Seró & Bisquert, 2010). The highest DSSC efficiency of 12.3% was achieved using a $Co^{2+/3+}$ based electrolyte with an organic dye combination (Hanewinkel, Knorr, Thomas, & Koch, 1997). Organic sensitizers are typically responsible for absorbing sunlight ranging from the UV region to the near infrared region of the spectrum, with a foremost efficiency of ~ 10.65 % for metal-free sensitizers (Obotowo, Obot, & Ekpe, 2016). The emerging solar cells have lower production costs, abundant materials, and simple processes. Accordingly, p-type organic semiconductors or organic hole-transport materials (HTMs) have been investigated, together with solvent free electrolyte, as potential substitutes for liquid electrolyte (Kojima, Teshima, Shirai, & Miyasaka, 2009; McDaniel, Fuke, Makarov, Pietryga, & Klimov, 2013; Zhao et al., 2011). Because of their outstanding optical properties (Cao et al., 2008), high extinction coefficients (Song, Cho, Lee, & Kang, 2014), and strong intrinsic dipole moments (Chae et al., 2014), inorganic sensitizers are preferable to organic dyes. Metal halide perovskites have gained considerable scientific attention due to their rapid evolution, revealing materials with remarkable optical, electrical, and mechanical characteristics (Heo et al., 2013; Jeng et al., 2013; Jeon et al., 2014; Wang et al., 2014).

The scientific breakthrough of the power conversion efficiency of hybrid organic–inorganic perovskite has now exceeded 25.8%, making it competitive with thin-film Photovoltaic (PV) technology (Min et al., 2021). Perovskite materials, both organic and inorganic, are among the most competitive absorbers for efficient solar cells. They have a low exciton bonding energy and a wide range of light absorption from visible to near infrared (Liu, Johnston, & Snaith, 2013; Wojciechowski, Saliba, Leijtens, Abate, & Snaith, 2014). Scanning Electrochemical Microscopy

(SEM) has proven to be an effective tool for investigating interfacial processes such as heterogeneous electron-transfer reactions (Ball, Lee, Hey, & Snaith, 2013), molecular transport across membranes (Noh, Im, Heo, Mandal, & Seok, 2013), adsorption/desorption processes (Zhu et al., 2014), corrosion processes (Hsu et al., 2014), the activity of living biological cells (Jeng et al., 2014), and charge transfer at liquid/liquid interfaces (Crossland et al., 2013). SEM was recently used to quantitatively investigate the electron transfer mechanism of nanoparticles put on an insulating surface. The ultramicroelectrode is positioned above the sensitive nanostructure oxide in the redox mediator at the UME in feedback mode (Alemu, Cui, et al., 2014; Alemu et al., 2015; Alemu, Zhang, et al., 2014; Alemu Getachew & Teketel, 2021; Getachew, 2022; Mengesha Tefashe, Nonomura, Vlachopoulos, Hagfeldt, & Wittstock, 2012; Shen, Nonomura, Schlettwein, Zhao, & Wittstock, 2006; Tefashe, Loewenstein, Miura, Schlettwein, & Wittstock, 2010; Zhang et al., 2014). In this study, we present a comparative study on the electrochemical microscopy investigation of the regeneration kinetics of organic dye C34/NiO and organmetallic sensitizer CH3NH3PbI3/NiO with an organic electrolyte of 1-methy-1H-tetrazole-5-thiolate (T-) with blue and red illumination.

2.EXPERIMENTAL METHODS

2.1. Materials

Chemicals

Organic isoperponal solvents, ethyl acetate alcohol, perovskites, NiO nanoparticles, nickel acetylacetonate, organic electrolyte T^-, organic dyes C343, and $CH_3NH_3PbI_3$ were all employed in this study. Figure 1 shows the chemical structures of (a) $CH_3NH_3PbI_3$, (b) C343, and (c) the electrolyte T^-.

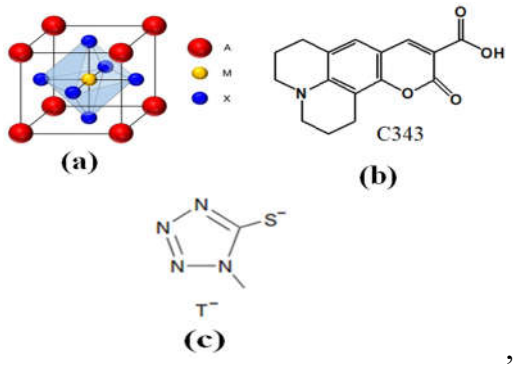


Figure 1. Chemical structure of (a) $CH_3NH_3PbI_3$, (b) C343, and (c) the electrolyte T^-

Nickel Oxide Films

The NiO nanoparticles (particle size ~20 nm) paste was prepared by ball-milled in ethanol with few droplets of acetate additive. Two pure ethyl cellulose (EC) powders, specifically EC (5–15mPas, 46070, Fluka) and EC (30–50mPas), were dissolved prior to usage in ethanol to yield 10 wt % solutions 4.5 g (EC (5–15 mPas) and 3.5 g EC (30–50 mPas)) of these 10 wt% ethanol mixtures were added to a round. The mixture of above colloidal solutions, ethyl cellulose (Aldrich) and terpinol were solicited and stirred alternatively to obtain a fine dispersion. A paste was made by evaporating the ethanol from the mixture on a rotary evaporator. FTO glass Nippon sheet glass, resistance 13 Ω/square were coated with nickel acetate ethanol solution (0.05M) by dip coating and subsequently dried before screen print. The photocathode films were screen-printed with the NiO paste and dried for 5min at 125ºC.This coating-drying procedure was repeated to obtain films with different thickness. The screen-printing technique was used to deposit NiO films consisting of nanoparticles on fluorine-doped tin oxide glass plates (FTO, Pilkington TEC15). The geometrical area of the NiO films was 4mm× 4 mm. The NiO electrodes were sintered under at 450ºC for 30 min with a ramping time of 30 min from room temperature 25ºC to 450 ºC, and then post-treated at 550 ºC for 15 min with a ramping time of 10 min from 450ºC to 550 ºC. After cooling down to room temperature, these films of NiO were kept in dye bath for 17–18h to obtain C343/NiO electrode. Then $CH_3NH_3PbI_3$/NiO electrode were prepared by the deposition of $CH_3NH_3PbI_3$ on the top of NiO films and sintering at 100ºC for 5 min (Alemu, Cui, et al., 2014; Alemu et al., 2015).

2.2. SECM Apparatus and Procedure

The SECM apparatus for dye-sensitized solar experiments were used. The SECM experiments were performed on a CHI920C electrochemical workstation (CH Instruments, Shanghai). The C343/NiO and NiO/$CH_3NH_3PbI_3$ electrodes were placed at the bottom of a small volume electrochemical cell and short-circuited by Pt wire to the electrolyte. The LEDs were placed close to the cell and focused on C343 dye-sensitized film by an objective lens of the photo-illuminated spot incident light power on the illuminated area of 0.0785cm^2 and photon flux density J_{hv} of the LEDs, blue and red, respectively, used as light sources in the experiment. SECM experiments were performed on the cell containing a Pt wire counter electrode and a 4mm diameter, 5cm high glass tube filled with a 10 mmol solution of $AgNO_3$ with supporting electrolyte 0.1mTBP as reference

electrode. The UME was RG~10, where RG is the ratio of the diameters of the glass sheath and the Pt wire. Before every experiment, UME was polished with 0.3mm of alumina powder and rinsed with water and ethanol. The electrodes are immersed in solution containing redox mediator with a sufficiently positive potential applied to the tip, electro-generated at a diffusion-controlled rate from solution species R to the UME. A 12.5µm radius Pt wire was sealed into a 5cm glass capillary vertical pull pin instrument (Figure 2a). The ultra-microelectrode (UME) was polished by a grinding instrument and micro-polishing cloth with 1.0, 0.3, and 0.05µm alumina powder (Figure2b). Then, the UME was sharpened conically to RG of 10, where RG is the ratio between the diameters of the glass sheath and the Pt disk. Figure 2(c and d) compares the cyclic voltammeter of a Pt electrode (d = 3 mm) and a Pt UME (d = 25 µm) in the 0.5mM $K_3Fe(CN)_6/K_4Fe(CN)_6$ with a scan rate of 50 mVs^{-1} (Alemu et al., 2015; Alemu Getachew & Teketel, 2021; Getachew, 2022; Mengesha Tefashe et al., 2012).

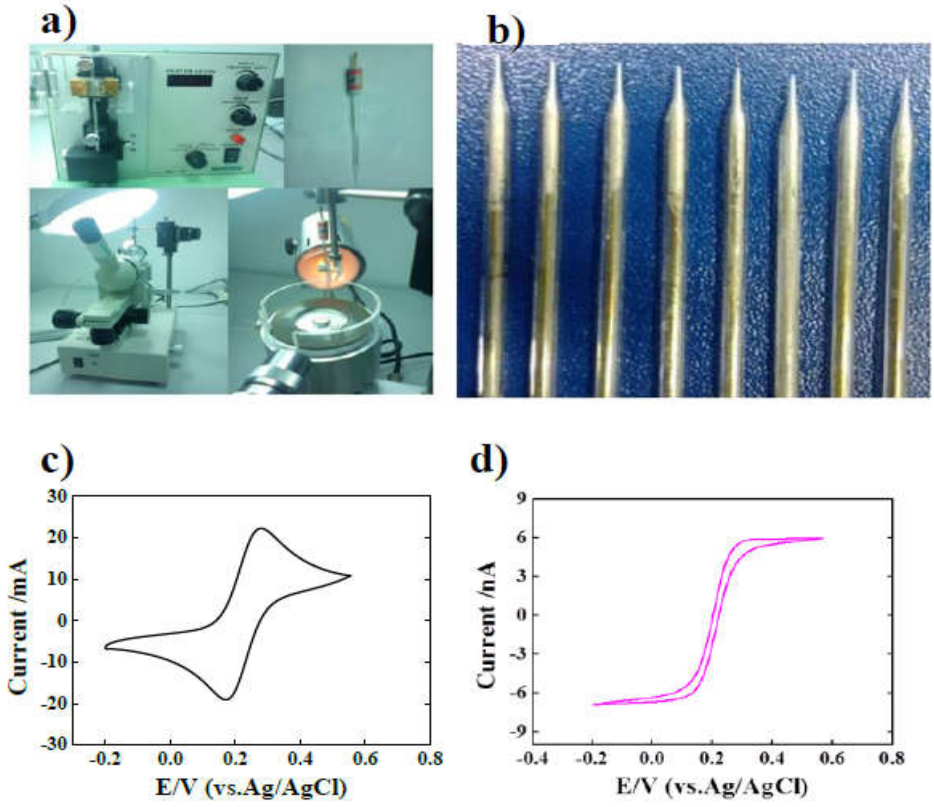


Figure 2. Optical images of (a) a grinding instrument (EG-400, Japan), (b) several ultra-microelectrodes (UME) with 25µm diameter Pt wire (Good fellow, Cambridge, UK) sealed into a 5 cm glass capillary. Cyclic voltammetry of (c) Pt electrode (d= 3 mm) and (d) Pt UME (d=25 µm) in 0.5mM $K_3Fe(CN)_6/K_4Fe(CN)_6$ with a scan rate of 50 mV s^{-1}(Alemu et al., 2015).

3. RESULTS AND DISCUSSION

In SECM feedback mode, the ultra-microelectrode (UME) serves as the working electrode in a three-electrode system. It is used to probe interfacial charge-transfer reactions by changing the faradic current flows at the tip. Upon illumination of the sensitizer, charge separation occurs when a hole is injected into the NiO valence band, and the C343 is reduced. In the case of the $CH_3NH_3PbI_3$/NiO film, under illumination, the photoexcitation generates electron–hole pairs. Figure 2(a and b) shows the cyclic voltammogram of an electrolyte in a solution at a Pt ultramicroelectrode. It illustrates an oxidation reaction wave at the UME and a reduction reaction wave at the electrode surface. Figure 2(c and d) shows the cyclic voltammeter at Pt UME (d=3 mm) and (d=25 μm) respectively in the 0.5mM $K_3Fe(CN)_6$/ $K_4Fe(CN)_6$ with a scan rate of $50mVs^{-1}$.

The UME current can be a steady-state current, as shown in Eqn. 1.

$$I_{T,\infty} = 4nCF\frac{k_{eff}}{\kappa}.r_T \quad (1)$$

Where $I_{T\infty}$ is the limited tip current on the UME, n is the number of electrons transferred at the tip of the UME, F is Faraday's constant, C is the concentration of reduced species, k_{eff} is the regeneration rate constant, r_T refer to the radius of the tip, and k denotes the normalized rate constant. The carrier's diffusion of electrons and the hole's movement in the contrary direction correspond to electric current. According to Licheng Sun.et studies, the suggested mechanisms of regeneration of the C343 dye sensitized NiO is as shown in Eqns. (2.1-2.5) (Cornut & Lefrou, 2008; Morandeira, Boschloo, Hagfeldt, & Hammarstrom, 2008; Morandeira, Boschloo, Hagfeldt, & Hammarström, 2005; Morandeira, Fortage, et al., 2008; Wei, Bard, & Mirkin, 1995). Furthermore, Eqns. (2.6-2.9) shows the illuminated $CH_3NH_3PbI_3$ sensitized NiO leading photo electrochemical reactions and at the surface of $CH_3NH_3PbI_3$ sensitized NiO (Anshebo & Gebreyohanes, 2022; Borgström et al., 2005; Gibson et al., 2012).

$$\mathrm{NiO}/C343 + \mathrm{hv} \longrightarrow \mathrm{NiO}/\mathrm{C}_{343}^{*} \longrightarrow \mathrm{C}_{343}^{-}/\mathrm{NiO} + \mathrm{h}_{\mathrm{Cb}}^{+} \quad (2.1)$$

$$\mathrm{C}_{343}^{-}/\mathrm{NiO} + \mathrm{h}_{\mathrm{Cb}}^{+} \longrightarrow \mathrm{NiO}/C343 \quad (2.2)$$

$$T_2 + 2S^{-} \longrightarrow 2\mathrm{T}^{\cdot} \quad (2.3)$$

$$\mathrm{C}_{343}^{-}/\mathrm{NiO} + \mathrm{T}^{\cdot} \longrightarrow \mathrm{NiO}/C343 + \mathrm{T}^{-} \quad (2.4)$$

$$T^{-} - 2\mathrm{e}^{-} \longrightarrow \mathrm{T}_2 \quad (2.5)$$

$$\mathrm{NiO}/\mathrm{CH_3NH_3PbI_3} + \mathrm{hv} \longrightarrow \mathrm{CH_3NH_3PbI_3}(\mathrm{h}^{+} + \mathrm{e}^{-}) \quad (2.6)$$

$$NiO/CH_3NH_3PbI_3\ (e^- + h^+) \xrightarrow{hv} NiO(h^+) + (e^-)CH_3NH_3PbI_3 \quad (2.7)$$

$$(e^- + h^+)CH_3NH_3PbI_3 \longrightarrow hv' \quad (2.8)$$

$$(e^- + h^+)CH_3NH_3PbI_3 \longrightarrow \nabla \quad (2.9)$$

To produce a reaction flux at the ultramicroelectrode (UME), in an electrolyte solution of 1-methy-1H-tetrazole-5-thiolate (T^-), the reaction stands for (Eqn. 2.3) at the UME NiO/sensitizer (Eqn. 2.4) and at the sensitized NiO surface (Eqn. 2.5). It is an illustrious example of electronic flux for hole transfers from $CH_3NH3PbI_3$ and C343 organic dyes to NiO. After charge injection from excited $CH_3NH3PbI_3$ and/or C343 to NiO oxides, there is a coupled reaction between the light harvester and the redox species that is produced on the UME.

In this study, SECM measurements were performed on the $CH_3NH_3PbI_3$ /NiO and $CH_3NH_3PbI_3$films both under blue and red illuminations. The experimental approach curves $I_T(z)$ were normalized to $I_T(L)$, and the normalized heterogeneous rate constants have been extracted by fitting them to an analytical approximation suggested by Cornut and Lefrou for a first-order reaction at the sample (Anshebo & Gebreyohanes, 2022; Borgström et al., 2005; Morandeira, Boschloo, et al., 2008; Morandeira et al., 2005).

$$I_T(L,k,RG) = I_T^{con}\left(L + \frac{1}{k}, RG\right) + \frac{I_T^{ins}(L,RG) - 1}{(1+2.47RG^{0.31}LK)\left(1+L^{0.006RG+0.133}k^{-0.0236RG+0.91}\right)} \quad (3)$$

Where, I_T^{con}, and I_T^{ins} are the normalized UME current, and the reaction at the sample is diffusion controlled, that are calculated according to the following equations, respectively.

$$I_T^{ins}(L,RG) = \frac{(2.08/RG^{0.358})\left(L - (0.145/RG)\right) + 1.585}{(2.08/RG^{0.358})(L + 0.0023RG) + 1.57 + (ln\, RG/L) + (2/\pi RG)ln\left(1 + (\pi RG/2L)\right)} \quad (3a)$$

$$I_T^{cond}(L + k^{-1}, RG) = \alpha(RG) + \frac{\pi}{4\beta(RG)\arctan(L + k^{-1})} + \left(\left(1 - \alpha(RG)\right) - \frac{1}{2\beta(RG)}\right)\frac{2}{\pi} arctan(L + k^{-1}) \quad (3b)$$

Where I_T^{ins} (L, RG) is the contribution of diffusion of T^- for the NiO electrode and diffusion of T_2 from solution to the UME. The rate of reaction at the surface of a sensitized sample is infinitely fast. For the sensitized NiO semiconductor sample, α(RG) and β(RG) are the constants. For the normalized, dimensionless constant obtained by fitting the experimental approach curves to the analytical approximations. Thus, regeneration rate constants k_{red} for the regeneration of the reduced sensitizer after injection of the hole into the valance band of a semiconductor at incident light of given intensity can be obtained from Eqn. 4 (Alemu, Cui, et al., 2014; Alemu et al., 2015).

$$k_{red} = \frac{2\, k_{eff}\, \Phi_{hv}\, J_{hv}}{3DL\Phi_{hv} - 6\, k_{eff}[T^-]} \qquad (4)$$

Where Γ_D is the surface concentration of the sensitizer in ground state, Φ_{hv} is the excitation cross section of adsorbed sensitizer and J_{hv} is the incident photon flux density.

Figure 3a shows the absorption spectra of $CH_3NH_3PbI_3$ and C343, and Figure 3b shows the relevant energy levels for FTO, NiO, $CH_3NH_3PbI_3$, C343 dye, and electrolyteT^-/T_2, which affect the regeneration kinetics rate.

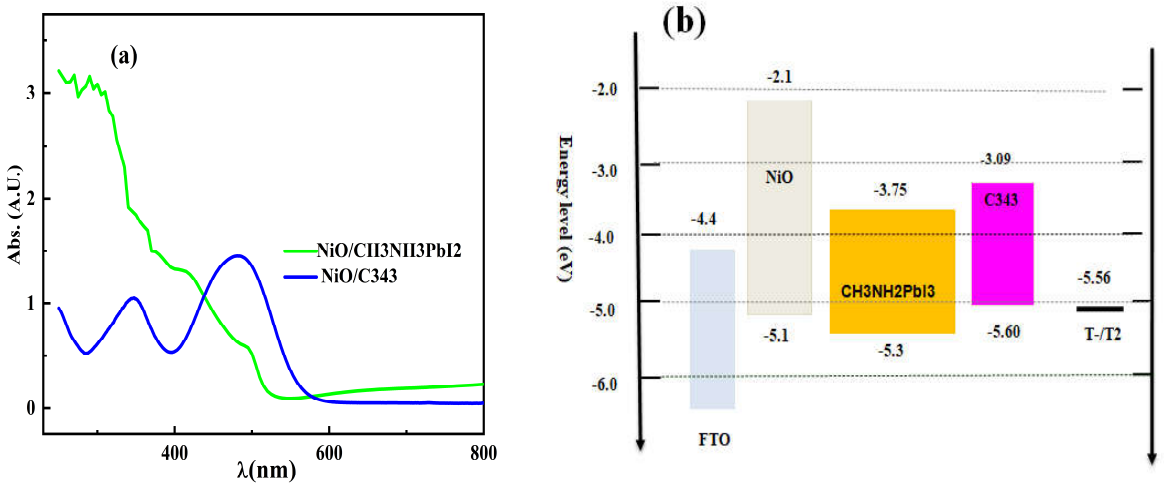


Figure 3.(a) The absorption spectrum of $CH_3NH_3PbI_3$, PEDOT and organic dyes C343 on NiO film (b) Energy-level-alignment diagram of the FTO, NiO, $MAPbI_3$, C343, and T^-/T_2,

Figure 4 illustrates SECM normalized approach curves of $CH_3NH_3PbI_3$/NiO and C343/NiO film in the T^- electrolyte under blue illumination. Figure.4a shows normalized approach curves toward $CH_3NH_3PbI_3$/NiO film under blue illumination with maximum wavelength of 490nm, for incident photon flux: J_{hv} increased from 2.2×10^{-9} to 22.4×10^{-9}molcm^{-2}s^{-1}(curve#1-7).

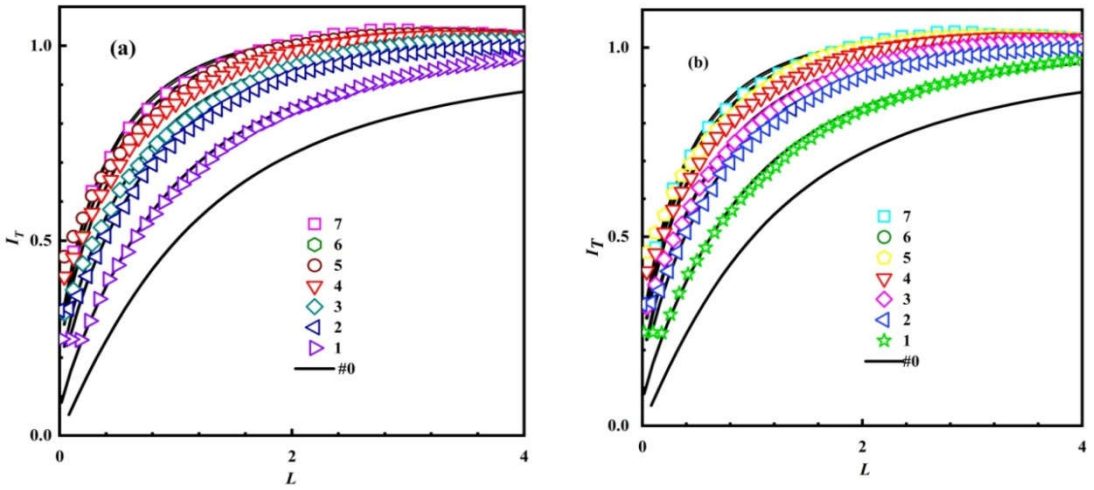


Figure 4. Normalized SECM feedback approach curves for the approach of a Pt disk electrode towards (a) NiO/$CH_3NH_3PbI_3$ and (b) C343/NiO sensitized film in the dark (curve #0) and under blue illumination.

When photon flux density increased and corresponding rate constant k_{eff} increased from 5.94×10^{-3}cms^{-1} to 16.9×10^{-3}cms^{-1} for $CH_3NH_3PbI_3$/NiO as shown (Table.1a). Figure 4b presents the normalized approach curve of C343/NiO film under blue illumination, J_{hv} increased from 2.2×10^{-9}cms^{-1} to 22.4×10^{-9}molcm^{-2}s^{-1}, k_{eff} increased from 3.99×10^{-3} cms^{-1} to 13.4×10^{-3}cms^{-1} (curve#1-7) as shown in Table.1b.

Table 1. Normalized heterogeneous rate constants k and the effective heterogeneous rate constants k_{eff} (cm s^{-1}) for the reduction of photo excited (a) NiO/$\mathbf{CH_3NH_3PbI_3}$ (b) NiO/C343 by T^- with different illumination intensities of blue LEDs. [T^-] = 1mM, D= 2.21×10^{-5} cm^2 s^{-1}, r_T =12.5 µm, RG =10, k_{eff} =kD/r_T

J_{hv} /10^{-9} [mol cm^{-2} s^{-1}]	Curve#	k	k_{eff}/10^{-3}(cms^{-1})
(a)NiO/$\mathbf{CH_3NH_3PbI_3}$			
22.4	7	0.0156	16.9
19.8	6	0.0152	16.5
13.9	5	0.0139	15.1
11.8	4	0.0132	14.3
6.82	3	0.0107	11.6
6.12	2	0.0101	11.0
2.20	1	0.0055	5.94
(b)NiO/C343			
22.4	7	0.0124	13.4
19.8	6	0.0119	12.9
13.9	5	0.0107	11.6
11.8	4	0.0101	10.9
6.82	3	0.0078	8.44
6.12	2	0.0073	7.96
2.20	1	0.0036	3.99

Figure 5 shows the SECM approach curves of UME toward (a) $CH_3NH_3PbI_3$/NiO (b) C343/NiO under red illumination. Figure.5a present normalized approach curves toward CH3NH3PbI3/NiO under red LED illumination. As photon flux density at J_{hv} increased from 2.10×10^{-9} to 14.6×10^{-9}molcm^{-2}s^{-1}, k_{eff} increased from 2.66×10^{-3}cms^{-1} to 8.96×10^{-3}cms^{-1} (Table.2a) (curve#1-7). Figure 5b presents the normalized approach curves toward C344/NiO under red LED illumination, k_{eff} increased from 1.54×10^{-3} to 4.38×10^{-3} cms^{-1} (Table.2b) (**curve#1-7**). Thus, the apparent heterogeneous rate constants k_{red} for the regeneration of the reduced dye (after injection the hole into the valance band of semiconductor) by the oxidized state of redox.

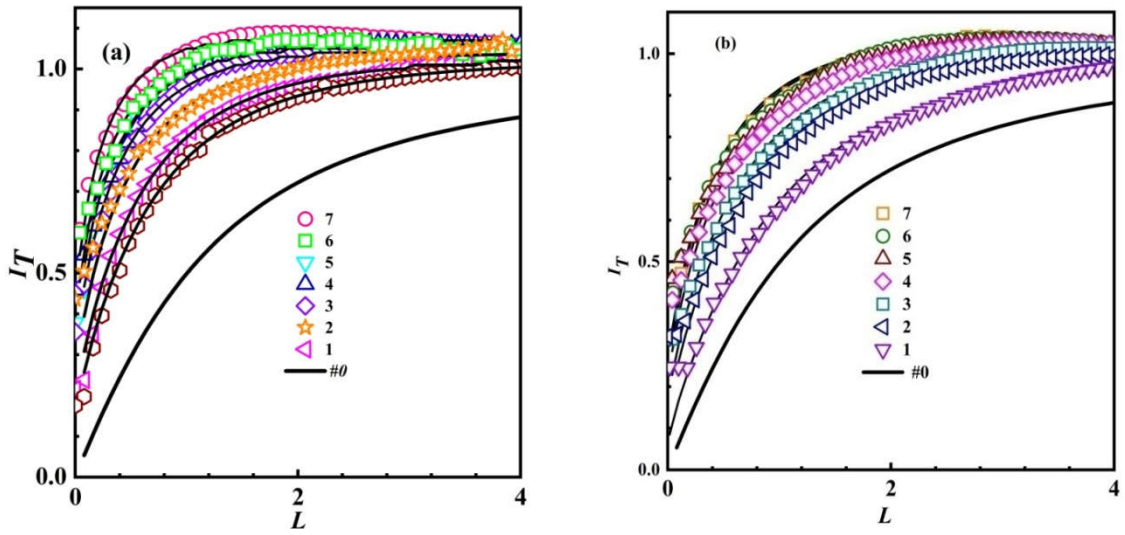


Figure 5. Normalized SECM feedback approach curves for the approach of a Pt disk electrode towards NiO/$CH_3NH_3PbI_3$ sensitized film in the dark (curve #0) and under illumination by a red LED.

The variation of k_{eff} with different intensities conform that the impact of light intensities on regeneration kinetics. Therefore, the rate constant of k_{red} for regeneration of the photo-excited sensitizer with redox at incident light intensity can be evaluated by using Equ. 4. The relationship between k_{eff} and J_{hv} for $CH_3NH_3PbI_3$/NiO and C343/NiO under blue LED illumination (maximum wavelength of 497nm) and red LED illumination (maximum wavelength of 647 nm) is illustrated in Figure 6.

Figure 6(a and b) shows experimental plot of k_{eff} vs $J_{hv}(\lambda)$ for $CH_3NH_3PbI_3$/NiO and C343/NiO film interfaces with electrolyte, T^-=1mM, with different intensities of blue and red LEDs. In both blue and red illuminations, k_{eff} of $CH_3NH_3PbI_3$/NiO is greater than the k_{eff} of C343/NiO. This confirms that the regeneration rate constant of $CH_3NH_3PbI_3$/NiO is significantly higher than that of the organic dye C343/NiO. As the $CH_3NH_3PbI_3$/NiO film exhibits the maximum photon absorption in the range of 560 nm to 800 nm in the visible region, the C343/NiO film only presents

maximum photon absorption at around 497 nm, as shown in Figure 3a. Thus, the apparent heterogeneous rate constants, $k_{red,}$ for the regeneration of the reduced sensitizer by the oxidized state of the redox shuttle after the injection of holes into the valance band of the semiconductor at a given incident light intensity can be obtained from Eqn.3. When illuminated, perovskite absorbs light and generates electron–hole pairs, and the exciton at the interface and remaining holes pass through across the perovskite layer. It enables perovskite $CH_3NH_3PbI_3$ act as both n- and p-type conductors, depending on the type of junction with a neighbouring semiconductor (Anshebo & Gebreyohanes, 2022; Borgström et al., 2005).

Table 2. Normalized heterogeneous rate constants k and the effective heterogeneous rate constants k_{eff} (cm s^{-1}) for the reduction of photo excited (a) NiO/$\mathbf{CH_3NH_3PbI_3}$ (b) NiO/C343 by T^- with different illumination intensities of red LEDs. [T^-] = 1mM, D= 2.21 × 10^{-5} cm^2 s^{-1}, r_T =12.5 µm, RG =10, k_{eff} =kD/r_T

J_{hv} /10^{-9} [mol cm^{-2} s^{-1}]	Curve#	*k*	k_{eff}/10^{-3}(cms^{-1})
(a)NiO/$\mathbf{CH_3NH_3PbI_3}$			
14.7	7	0.0085	8.96
13.1	6	0.0082	8.55
12.1	5	0.0074	8.26
9.44	4	0.0071	7.35
6.82	3	0.0054	6.16
4.20	2	0.0051	4.52
2.10	1	0.0026	2.66
(b) NiO/C343			
14.7	7	0.0064	4.38
13.1	6	0.0062	4.22
12.1	5	0.0055	4.11
9.44	4	0.0052	3.74
6.82	3	0.0041	3.23
4.20	2	0.0039	2.47
2.10	1	0.0021	1.54

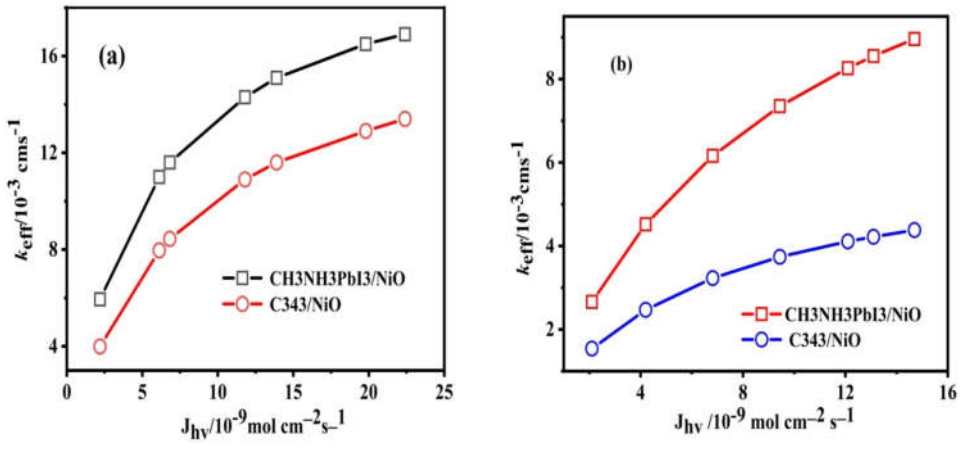


Figure 6. Plot of experimental values of *k*eff vs. J_{hv}. The lines represent the fitting of k_{eff} according to Eqn. 2 with k_{red} and ϕ_{hv} as adjustable parameters for $CH_3NH_3PbI_3$/NiO (□) C343/NiO (∘) (a) in blue illumination, (b) in red illumination

Therefore, the kinetic rate constant, k_{red}, and excitation cross section, Φ_{hv}, for the $CH_3NH_3PbI_3$/NiO film were evaluated to be k_{red} =9.98×10^6 mol^{-1}cm^3 s^{-1}, Φ_{hv}= 6.87×10^6 mol cm^2 in blue LED illumination, and Φ_{hv} = 4.89×10^6 mol cm^2 in red LED illumination. Moreover, for the C343/NiO film, k_{red}=4.51×10^5 mol^{-1} cm^{3}s^{-1}, Φ_{hv}=3.56×10^5 mol cm^2 in blue LED illumination, and Φ_{hv}=2.15×10^5 mol cm^2 in red LED illumination, were evaluated as shown in Table 3 (Gibson et al., 2012; Odobel, Le Pleux, Pellegrin, & Blart, 2010). The apparent heterogeneous rate constants, k_{red}, and excitation cross section of the organometalic sensitizer ($CH_3NH_3PbI_3$ /NiO) film were significantly higher than those of organic dyes (C343/NiO) in blue LED illumination. In red illumination, the excitation crosssection of the inorganic sensitizer film was significantly higher than that of organic dyes. This result confirms that the absorption coefficient of $CH_3NH_3PbI_3$/NiO in the visible region is much higher than of C343/NiO (Eames et al., 2015; Patois, Lakard, Martin, & Fievet, 2010). Many scientific studies require knowledge of the organometallic sensitizer ($CH_3NH_3PbI_3$) excitation cross section, which is very useful for $CH_3NH_3PbI_3$ applications such as solar cells. The distinct optical properties of sensitizer ($CH_3NH_3PbI_3$), such as broad absorption spectral range, high extinction coefficient, ambipolar diffusion, and long carrier diffusion length, are advantages. These qualities allow the organometallic perovskite to absorb light better than organic dyes for DSCs and other thin-film photovoltaics.

Table 3. Fitting results of regeneration rate and cross section from k_{eff} vs. J_{hv} for various substrates

NiO/substrate	**LED**	k_{red} **(mol^{-1}cm^{3}s^{-1})**	Φ_{hv}**(cm^2 mol^{-1})**
$CH_3NH_3PbI_3$	Blue	9.98×10^6	6.87×10^6
	Red		4.89×10^6
C343	Blue	4. 51×10^5	3.56×10^5
	Red		2.31×10^5

CONCLUSION

The kinetics of the regeneration of the light absorbing sensitizer molecules by the organic electrolyte 1-methy-1H-tetrazole-5-thiolate (T^-) were investigated by using the feedback mode of scanning electrochemical microscopy (SECM). The regeneration rate constants were extracted from the approach curves. We obtained that the regeneration parameters of organometallic perovskite, such as the reduction rate constant (k_{red}), the absorption cross section (Φ_{hv}), and the regeneration rate constant (k_{eff}), were significantly higher than the organic dye. As a result, the

regeneration kinetics of an organometallic sensitizer are more than hundred times faster than the regeneration kinetics of an organic dye. The use of SECM feedback modes to describe regeneration parameters, reduction constants, and absorption cross-sections has proven to be a novel procedure. Therefore, the overall SECM investigation opens a new outlook for p-type dye-sensitized solar cell characterization.

CONFLICTS OF INTEREST

The authors declare that they have no conflicts of interest.

ACKNOWLEDGMENTS

The experiments were performed on a CHI920C electrochemical workstation (CH Instruments, Shanghai) provided by the Chinese Scholarship Council (CSC) for Ph.D. fellowship.

REFERENCES

Alemu, Cui, J., Cao, K., Li, J., Shen, Y., & Wang, M. (2014). Investigation of the regeneration kinetics of organic dyes with pyridine ring anchoring groups by scanning electrochemical microscopy. *RSC advances, 4*(93), 51374-51380.

Alemu, Li, J., Cui, J., Xu, X., Zhang, B., Cao, K., . . . Wang, M. (2015). Investigation on regeneration kinetics at perovskite/oxide interface with scanning electrochemical microscopy. *Journal of Materials Chemistry A, 3*(17), 9216-9222.

Alemu, Zhang, B., Li, J., Xu, X., Cui, J., Shen, Y., & Wang, M. (2014). Investigation of dye-regeneration kinetics at dye-sensitized p-type CuCrO 2 film/electrolytes interface with scanning electrochemical microscopy. *Nano, 9*(05), 1440008.

Alemu Getachew, & Teketel, A. (2021). Dye regeneration kinetics of sensitized nickel oxide films under illumination investigated by scanning electrochemical microscopy. *Advances in Materials Physics and Chemistry, 11*(04), 78-92.

Anshebo, G. A., & Gebreyohanes, A. A. (2022). Investigation on dye regeneration kinetics at P-type sensitized nanoparticle nickel oxide film by scanning electrochemical microscopy. *Journal of Nanomaterials, 2022*.

Ball, J. M., Lee, M. M., Hey, A., & Snaith, H. J. (2013). Low-temperature processed meso-superstructured to thin-film perovskite solar cells. *Energy & Environmental Science, 6*(6), 1739-1743.

Borgström, M., Blart, E., Boschloo, G., Mukhtar, E., Hagfeldt, A., Hammarström, L., & Odobel, F. (2005). Sensitized hole injection of phosphorus porphyrin into NiO: toward new photovoltaic devices. *The Journal of Physical Chemistry B, 109*(48), 22928-22934.

Cao, Y., Zhang, J., Bai, Y., Li, R., Zakeeruddin, S. M., Grätzel, M., & Wang, P. (2008). Dye-sensitized solar cells with solvent-free ionic liquid electrolytes. *The Journal of Physical Chemistry C, 112*(35), 13775-13781.

Chae, H., Song, D., Lee, Y.-G., Son, T., Cho, W., Pyun, Y. B., . . . Bisquert, J. (2014). Chemical effects of tin oxide nanoparticles in polymer electrolytes-based dye-sensitized solar cells. *The Journal of Physical Chemistry C, 118*(30), 16510-16517.

Chen, C.-Y., Wang, M., Li, J.-Y., Pootrakulchote, N., Alibabaei, L., Ngoc-le, C.-h., . . . Wu, C.-G. (2009). Highly efficient light-harvesting ruthenium sensitizer for thin-film dye-sensitized solar cells. *ACS nano, 3*(10), 3103-3109.

Cornut, R., & Lefrou, C. (2008). New analytical approximation of feedback approach curves with a microdisk SECM tip and irreversible kinetic reaction at the substrate. *Journal of Electroanalytical Chemistry, 621*(2), 178-184.

Crossland, E. J., Noel, N., Sivaram, V., Leijtens, T., Alexander-Webber, J. A., & Snaith, H. J. (2013). Mesoporous TiO2 single crystals delivering enhanced mobility and optoelectronic device performance. *nature, 495*(7440), 215-219.

Eames, C., Frost, J. M., Barnes, P. R., O'regan, B. C., Walsh, A., & Islam, M. S. (2015). Ionic transport in hybrid lead iodide perovskite solar cells. *Nature communications, 6*(1), 7497.

Getachew, A. A. (2022). Dye regeneration kinetics of C343-sensitized nickel oxide investigated by scanning electrochemical microscopy. *Materials Sciences and Applications, 13*(1), 22-38.

Gibson, E. A., Le Pleux, L., Fortage, J., Pellegrin, Y., Blart, E., Odobel, F., . . . Boschloo, G. (2012). Role of the triiodide/iodide redox couple in dye regeneration in p-type dye-sensitized solar cells. *Langmuir, 28*(15), 6485-6493.

Grätzel, M. (2003). Dye-sensitized solar cells. *Journal of photochemistry and photobiology C: Photochemistry Reviews, 4*(2), 145-153.

Hagfeldt, A., & Graetzel, M. (1995). Light-induced redox reactions in nanocrystalline systems. *Chemical reviews, 95*(1), 49-68.

Hanewinkel, B., Knorr, A., Thomas, P., & Koch, S. (1997). Optical near-field response of semiconductor quantum dots. *Physical Review B, 55*(20), 13715.

Haque, S. A., Palomares, E., Cho, B. M., Green, A. N., Hirata, N., Klug, D. R., & Durrant, J. R. (2005). Charge separation versus recombination in dye-sensitized nanocrystalline solar cells: the minimization of kinetic redundancy. *Journal of the American Chemical Society, 127*(10), 3456-3462.

Heo, J. H., Im, S. H., Noh, J. H., Mandal, T. N., Lim, C.-S., Chang, J. A., . . . Nazeeruddin, M. K. (2013). Efficient inorganic–organic hybrid heterojunction solar cells containing perovskite compound and polymeric hole conductors. *Nature photonics, 7*(6), 486-491.

Hsu, H. Y., Wang, C. Y., Fathi, A., Shiu, J. W., Chung, C. C., Shen, P. S., . . . Diau, E. W. G. (2014). Femtosecond excitonic relaxation dynamics of perovskite on mesoporous films of Al2O3 and NiO nanoparticles. *Angewandte Chemie, 126*(35), 9493-9496.

Jeng, J. Y., Chen, K. C., Chiang, T. Y., Lin, P. Y., Tsai, T. D., Chang, Y. C., . . . Hsu, Y. J. (2014). Nickel oxide electrode interlayer in CH3NH3PbI3 perovskite/PCBM planar-heterojunction hybrid solar cells. *Advanced materials, 26*(24), 4107-4113.

Jeng, J. Y., Chiang, Y. F., Lee, M. H., Peng, S. R., Guo, T. F., Chen, P., & Wen, T. C. (2013). CH3NH3PbI3 perovskite/fullerene planar-heterojunction hybrid solar cells. *Advanced materials, 25*(27), 3727-3732.

Jeon, N. J., Lee, H. G., Kim, Y. C., Seo, J., Noh, J. H., Lee, J., & Seok, S. I. (2014). o-Methoxy substituents in spiro-OMeTAD for efficient inorganic–organic hybrid perovskite solar cells. *Journal of the American Chemical Society, 136*(22), 7837-7840.

Kojima, A., Teshima, K., Shirai, Y., & Miyasaka, T. (2009). Organometal halide perovskites as visible-light sensitizers for photovoltaic cells. *Journal of the American Chemical Society, 131*(17), 6050-6051.

Liu, M., Johnston, M. B., & Snaith, H. J. (2013). Efficient planar heterojunction perovskite solar cells by vapour deposition. *nature, 501*(7467), 395-398.

Mathew, S., Yella, A., Gao, P., Humphry-Baker, R., Curchod, B. F., Ashari-Astani, N., . . . Grätzel, M. (2014). Dye-sensitized solar cells with 13% efficiency achieved through the molecular engineering of porphyrin sensitizers. *Nature chemistry, 6*(3), 242-247.

McDaniel, H., Fuke, N., Makarov, N. S., Pietryga, J. M., & Klimov, V. I. (2013). An integrated approach to realizing high-performance liquid-junction quantum dot sensitized solar cells. *Nature communications, 4*(1), 2887.

Mengesha Tefashe, U., Nonomura, K., Vlachopoulos, N., Hagfeldt, A., & Wittstock, G. (2012). Effect of cation on dye regeneration kinetics of N719-sensitized TiO2 films in acetonitrile-based and ionic-liquid-based electrolytes investigated by scanning electrochemical microscopy. *The Journal of Physical Chemistry C, 116*(6), 4316-4323.

Min, H., Lee, D. Y., Kim, J., Kim, G., Lee, K. S., Kim, J., . . . Kim, M. G. (2021). Perovskite solar cells with atomically coherent interlayers on SnO2 electrodes. *nature, 598*(7881), 444-450.

Mora-Seró, I., & Bisquert, J. (2010). Breakthroughs in the development of semiconductor-sensitized solar cells. *The journal of physical chemistry letters, 1*(20), 3046-3052.

Morandeira, A., Boschloo, G., Hagfeldt, A., & Hammarstrom, L. (2008). Coumarin 343− NiO films as nanostructured photocathodes in dye-sensitized solar cells: ultrafast electron transfer, effect of the I3−/I− redox couple and mechanism of photocurrent generation. *The Journal of Physical Chemistry C, 112*(25), 9530-9537.

Morandeira, A., Boschloo, G., Hagfeldt, A., & Hammarström, L. (2005). Photoinduced ultrafast dynamics of coumarin 343 sensitized p-type-nanostructured NiO films. *The Journal of Physical Chemistry B, 109*(41), 19403-19410.

Morandeira, A., Fortage, J., Edvinsson, T., Le Pleux, L., Blart, E., Boschloo, G., . . . Odobel, F. (2008). Improved photon-to-current conversion efficiency with a nanoporous p-type NiO electrode by the use of a sensitizer-acceptor dyad. *The Journal of Physical Chemistry C, 112*(5), 1721-1728.

Noh, J. H., Im, S. H., Heo, J. H., Mandal, T. N., & Seok, S. I. (2013). Chemical management for colorful, efficient, and stable inorganic–organic hybrid nanostructured solar cells. *Nano letters, 13*(4), 1764-1769.

O'regan, B., & Grätzel, M. (1991). A low-cost, high-efficiency solar cell based on dye-sensitized colloidal TiO2 films. *nature, 353*(6346), 737-740.

Obotowo, I., Obot, I., & Ekpe, U. (2016). Organic sensitizers for dye-sensitized solar cell (DSSC): Properties from computation, progress and future perspectives. *Journal of Molecular Structure, 1122*, 80-87.

Odobel, F., Le Pleux, L., Pellegrin, Y., & Blart, E. (2010). New photovoltaic devices based on the sensitization of p-type semiconductors: challenges and opportunities. *Accounts of chemical research, 43*(8), 1063-1071.

Patois, T., Lakard, B., Martin, N., & Fievet, P. (2010). Effect of various parameters on the conductivity of free standing electrosynthesized polypyrrole films. *Synthetic Metals, 160*(19-20), 2180-2185.

Shen, Y., Nonomura, K., Schlettwein, D., Zhao, C., & Wittstock, G. (2006). Photoelectrochemical kinetics of eosin y-sensitized zinc oxide films investigated by scanning electrochemical microscopy. *Chemistry, 12*(22), 5832-5839. doi:10.1002/chem.200501241

Song, D., Cho, W., Lee, J. H., & Kang, Y. S. (2014). Toward higher energy conversion efficiency for solid polymer electrolyte dye-sensitized solar cells: ionic conductivity and TiO2 pore-filling. *The journal of physical chemistry letters, 5*(7), 1249-1258.

Tefashe, U. M., Loewenstein, T., Miura, H., Schlettwein, D., & Wittstock, G. (2010). Scanning electrochemical microscope studies of dye regeneration in indoline (D149)-sensitized ZnO photoelectrochemical cells. *Journal of Electroanalytical Chemistry, 650*(1), 24-30.

Tributsch, H., & Calvin, M. (1971). Electrochemistry of excited molecules: photo-electrochemical reactions of chlorophylls. *Photochemistry and Photobiology, 14*(2), 95-112.

Wang, Ball, J. M., Barea, E. M., Abate, A., Alexander-Webber, J. A., Huang, J., . . . Snaith, H. J. (2014). Low-temperature processed electron collection layers of graphene/TiO2 nanocomposites in thin film perovskite solar cells. *Nano letters, 14*(2), 724-730.

Wang, Grätzel, C., Zakeeruddin, S., & Grätzel, M. (2012). Recent developments in redox electrolytes for dye-sensitized solar cells. *Energy & Environmental Science, 5*(11), 9394-9405.

Wei, C., Bard, A. J., & Mirkin, M. V. (1995). Scanning electrochemical microscopy. 31. Application of SECM to the study of charge transfer processes at the liquid/liquid interface. *The Journal of Physical Chemistry, 99*(43), 16033-16042.

Wojciechowski, K., Saliba, M., Leijtens, T., Abate, A., & Snaith, H. J. (2014). Sub-150 C processed meso-superstructured perovskite solar cells with enhanced efficiency. *Energy & Environmental Science, 7*(3), 1142-1147.

Yella, A., Lee, H.-W., Tsao, H. N., Yi, C., Chandiran, A. K., Nazeeruddin, M. K., . . . Grätzel, M. (2011). Porphyrin-sensitized solar cells with cobalt (II/III)–based redox electrolyte exceed 12 percent efficiency. *Science, 334*(6056), 629-634.

Zhang, B., Xu, X., Zhang, X., Huang, D., Li, S., Zhang, Y., . . . Chen, W. (2014). Investigation of dye regeneration kinetics in sensitized solar cells by scanning electrochemical microscopy. *ChemPhysChem, 15*(6), 1182-1189.

Zhao, J., Shen, X., Yan, F., Qiu, L., Lee, S., & Sun, B. (2011). Solvent-free ionic liquid/poly (ionic liquid) electrolytes for quasi-solid-state dye-sensitized solar cells. *Journal of Materials Chemistry, 21*(20), 7326-7330.

Zhu, Z., Bai, Y.-L., Zhang, L., Sun, D., Fang, J., & Zhu, S. (2014). Two nanocage anionic metal–organic frameworks with rht topology and {[M (H 2 O) 6] 6} 12+ charge aggregation for rapid and selective adsorption of cationic dyes. *Chemical Communications, 50*(93), 14674-14677.

Publisher's Note

Daagu International Journal of Basic and Applied Research remains neutral with regard to jurisdictional claims in published maps and institutional affiliations.